Title
LAVES PHASE PRECIPITATION IN Fe-Ta ALLOTS

Authors
Jones, Russell H.
Zackay, V.F.
Parker, E.R.

Publication Date
1972-10-01

Submitted to
Metallurgical Transactions

LBL-110
Preprint

LAVES PHASE PRECIPITATION IN Fe-Ta ALLOYS

Russell H. Jones, V. F. Zackay and E. R. Parker

October 1972

Prepared for the U.S. Atomic Energy Commission
under Contract W-7405-ENG-48

DISCLAIMER

LBL-110

LAVES PHASE PRECIPITATION IN Fe-Ta ALLOYS

Russell H. Jones, V. F. Zackay and E. R. Parker

Inorganic Materials Research Division, Lawrence Berkeley Laboratory and Department of Materials Science and Engineering, College of Engineering; University of California, Berkeley, California

ABSTRACT

The age-hardening characteristics of iron-tantalum alloys have been been studied by means of optical and transmission electron microscopy, X-ray diffraction, electron beam microprobe analysis and scanning electron microscopy.

These studies suggest that Fe_2Ta is isomorphous with the structure type, $MgZn_2$, (C14) and that the compound Fe_2Ta has a range of homogeneity. The latter results correspond with the predictions of the Engel-Brewer correlation. Also, it has been found that precipitation occurred in the following sequence: grain boundaries, dislocation, then matrix. A $(110)_\alpha$ habit plane is favored for the precipitation of the hexagonal Laves phase in iron, but a $(100)_\alpha$ habit plane was observed in the Fe-Ta alloys investigated. It was concluded that particles with a $(100)_\alpha$ habit plane formed by an auto-catalytic dislocation precipitation mechanism.

Uniaxial tensile tests were made of age-hardened Fe-Ta alloys. Failure occurred by transgranular cleavage which had initiated in the grain boundary.

INTRODUCTION

The development of iron base alloys with a low alloy content for elevated temperature service is a desirable goal. An iron base alloy hardened by particles of an intermetallic compound rather than a carbide could possibly have useful low temperature or elevated temperature properties. It is known that interstitial elements in iron raise the ductile-brittle transition, so an iron base alloy with low carbon, nitrogen and oxygen contents could have good ductility at low temperatures. Also, an intermetallic compound would have greater stability at elevated temperatures than a carbide. The Laves phase is known to be a hard compound which would be an effective obstacle to dislocation motion. However, the age hardening characteristics of iron base alloys hardened primarily by the Laves phase have not been fully determined. Precipitation of the Laves phase from supersaturated α-iron in the Fe-Be, Fe-Nb, Fe-Ti and Fe-W systems has been reviewed by Hornbogen,[1] and a recent investigation[2] of the Fe-Mo system showed that Fe_2Mo was the stable phase in equilibrium with α-iron up to about 950°C. Laves phase precipitation from α-iron supersaturated with tantalum have not been reported; however, precipitation in the Fe-Nb system, which is similar, has been studied by Speich.[3]

The ability of a second phase to impede dislocation motion results in Orowan type hardening when the interparticle spacing is greater than some critical value. The flow properties of the particle are also important because the stresses resulting from dislocation tangles around the particle can cause fracture or flow in the particle or possibly interface failure. The Laves phase has generally been characterized as a

brittle compound. However, studies by G. Sasaki[4] of the region around a microhardness indention in the Laves phases Fe_2Nb, Fe_2Ta, Fe_2Ti, Fe_2Zr and Fe_2Hf have shown Fe_2Ta to be the most ductile of these compounds. The combination of a second phase which will impede matrix dislocations but will flow rather than fracture at higher stress levels makes the Fe-Ta system look attractive as an age hardening system.

Structural studies of precipitation in the Fe-Ta system have been undertaken because of the small amount of information available concerning this system, the attractive properties of the Fe_2Ta compound, the low alloy contents required for hardening, and the oxidation resistance imparted by the tantalum.

EXPERIMENTAL PROCEDURE

The alloys for this study were prepared from 99.95% purity electrolytic iron and 99.9% purity 0.1875 in diameter tantalum rod. The alloys were melted and cast in a vacuum induction furnace under an argon atmosphere. The 1.250 in. diameter ingots were form rolled at 950°C into 0.50 in. square rods. Specimens encapsulated in quartz and solution treated at 1400°C for 1 hour were brine quenched and subsequently aged in a molten salt bath.

Hardness tests were made with a Leitz Mini load hardness tester using a Vickers indentor with 2 kg load. After heat treatment the specimens were metallographically polished and etched prior to hardness testing. The mechanical properties were determined using an Instron tensile testing machine at a strain rate of 4×10^{-3}/min with 0.250 in. nominal diameter tensile specimens (ASTM Designation E8-65T). The fracture surfaces of the failed tensile specimens were examined with a JEOL scanning electron microscope.

The precipitate morphology was studied with carbon extraction replicas and thin foils by means of an Hitachi HU-125 electron microscope at 100 KV. The replicas were extracted in an acetic 10% perchloic acid solution with 25 volts applied across the sample and a stainless steel cathode. Thin foils were prepared by surface grinding to 0.010 in., chemical thinning to 0.002 in. with a solution of 85 parts H_2O_2, 10 parts H_2O and 5 parts HF, and jet polishing in an acetic 10% perchloic solution at 18°C.

X-ray diffraction patterns of Fe_2Ta particles were obtained with an 11.46 cm diameter Debye-Scherrer camera and Cr K_α radiation, with the

film loaded in the Straumanis position. The line intensities were measured from the film with a Jarrell-Ash recording microphotometer. The Laves phase particles were obtained by dissolving an overaged 2 at. pct Ta iron alloy in a 10% nitric acid solution. The change in the lattice parameter of iron with solute content was measured by means of a Norelco X-ray diffractometer using Cu K_α radiation and with a crystal monochrometer designed to reduce the flourescent iron radiation.

DISCUSSION OF RESULTS

A. Fe-Ta Phase Relationships

Binary alloy of iron-niobium and iron-tantalum have many similarities as the phase diagrams given by Elliott[5] and Hansen[6] indicate. A major difference between these two diagrams is the composition range of 58-78 at. pct iron at 1000°C for Fe_2Nb; whereas, no composition range is shown for Fe_2Ta. This indicated difference is questionable because of the similarities between the niobium and tantalum atoms, and because of theoretical work on phase stability by L. Brewer.[7] Brewer indicated that a stability range of about 10 at. pct exists for Fe_2Ta at 1200°C. The most recent phase diagram for the Fe-Ta system has been published by Sinha and Hume-Rothery[8] and is shown in Fig. 1. The maximum solubility of tantalum in iron occurs in the δ phase at 1440°C ± 2 and is reported[8] to be 2.8 at. pct. The δ phase decomposes eutectoidally at 1293°C ± 3 by the following reaction:

$$\delta(1.1 \text{ at. pct Ta}) = \gamma(0.5 \text{ at. pct Ta}) + Fe_2Ta$$

and the γ phase decomposes peritectoidally at 974°C ± 3 by the following reaction:

$$Fe_2Ta + \gamma(0.3 \text{ at. pct Ta}) = \alpha(0.6 \text{ at. pct Ta})$$

The solubility of tantalum in α-iron decreases with temperature from the maximum at 974°C, but the solvus curve has not been determined.

B. Morphology and Kinetics of the Allotropic Transformations

The solubility of tantalum in α-iron decreases with temperature which makes age-hardening attainable. However, the desired degree of hardening

could not be obtained by solution treating in the α phase region because of the low tantalum solubility. Because of this limitation, the δ phase field was utilized for solution treatment. The structure which resulted after quenching from the δ phase field was either retained δ or massive α which resulted from the $\delta \rightarrow \gamma \rightarrow \alpha$ transformation sequence.

The occurrence of the $\delta \rightarrow \gamma$ transformation was detected by examining the grain structure of a metallographically polished sample. Also, X-ray diffraction was used to determine the crystal structure of the product phase, and in all cases the room temperature structure was BCC. When no transformation had occurred, the grain size was about 1 mm diameter with an equiaxed grain shape, but regions which had undergone the $\delta \rightarrow \gamma \rightarrow \alpha$ transformation had irregular acicular boundaries which are typical of the massive α transformation in iron.

The morphology of the γ and α phases is clearly demonstrated by the 1 at. pct Ta alloy which had undergone partial transformation during quenching, as seen in Fig. 2 and Fig. 3. Using the Dube morphological classification system,[9] the structure in Fig. 2a can be identified as grain boundary allotriomorphs and intragranular idiomorphs and that in Fig. 3 as a primary saw tooth structure. Aaronson[10] has shown that in Fe-C systems proeutectoid ferrite forms with similar morphologies, and these morphologies have also been observed for primary phases as well as intermetallic compounds in other alloy systems.[11] It has also been shown that as a function of grain misorientation the tendency is to form grain boundary allotriomorphs at large misorientations, primary sawteeth at intermediate, and primary sideplates at small misorientations. The lack of low angle boundaries in the Fe-Ta system after a solution anneal

of 1 hour at 1400°C resulted in the γ phase appearing only as primary sawteeth or grain boundary allotriomorphs.

The interface between the grain boundary allotriomorphs, idiomorphs and sawteeth and the prior δ phase have been outlined by the precipitation of Fe_2Ta. Precipitation has also occurred at the prior δ boundaries and the massive α boundaries within a prior γ grain. In most cases the grain boundary allotriomorph has grown into adjacent grains by equal amounts, with straight boundaries in both grains or only one grain. The structure of these straight boundaries may be dislocation type or intermediate between dislocation type and disordered. Of the four boundaries surrounding the grain shown in Fig. 2b it is improbable that more than one is a dislocation boundary because the crystallographic orientation relationship of the one dislocation boundary would restrict the interfacial match up between the other interfaces. The primary sawtooth boundaries are subject to the same constraint, so that only one of the boundaries in Fig. 3 may be dislocation type.

The irregular boundaries resulting from the $\gamma \rightarrow \alpha$ transformation, easily identified in Fig. 2b, were always observed whenever the $\delta \rightarrow \gamma$ transformation had occurred. Alloys which did not undergo the $\delta \rightarrow \gamma \rightarrow \alpha$ transformation had a quenched structure which could be described as a retained BCC structure with Fe_2Ta precipitates at the grain boundaries. The structure of those which did undergo this transformation could be described as a mixture of massive α and retained δ with Fe_2Ta precipitates at the δ, γ and α boundaries. Laves phase particles at a retained δ boundary are shown in Fig. 4. Electron microscope investigations also revealed a low dislocation density in the retained δ phase.

Schematic TTT curves for hypoeutectoid and hypereutectoid compositions have been constructed from structural studies of quenched samples. The transformation curve for a hypoeutectoid composition is shown in Fig. 5a. The $\delta + \gamma + Fe_2Ta$ nose is shifted to longer times than the $\delta + \gamma$ nose because it was observed that all the hypoeutectoid alloys had either partially or completely undergone the $\delta \rightarrow \gamma \rightarrow \alpha$ transformation, while no matrix precipitation was detected. Examination of the quenched structure cannot reveal whether the $\delta \rightarrow \gamma$ transformation occurred completely above the eutectoid temperature. Therefore, it is not known how close the $\delta + \gamma$ curve and $\delta + \gamma + Fe_2Ta$ curve lie below the eutectoid temperature. The lack of matrix precipitation of the Laves phase during quenching was confirmed by electron microscopy of 1 at. pct and 2 at. pct Ta alloys and lattice parameter versus solute content measurements. A plot of the lattice parameter versus tantalum content for the Fe-Ta system has a slope very similar to that of the Fe-Nb system[12], as shown in Fig. 6. This indicates that the tantalum was still in solution after quenching. In hypereutectoid alloys neither the $\delta \rightarrow \gamma \rightarrow \alpha$ transformation or matrix precipitation were detected after quenching. In Fig. 5b the $\delta + Fe_2Ta$ curve is placed at shorter times than the $\delta + \gamma + Fe_2Ta$ curve because of the lack of observance of the $\delta \rightarrow \gamma$ transformation.

C. Morphology and Kinetics of Laves Phase Precipitation

1) Age Hardening Characteristics: The hardness versus solute content in Fe-Nb and Fe-Ti alloys was investigated by Speich[3] and it showed a linear dependence with solute content. The as-quenched hardness of 1 at. pct and 2 at. pct tantalum samples with the retained δ structure fit this relationship, as shown in Fig. 7. The hardness of a 2.3 at. pct

niobium sample tested by Speich showed a deviation from the expected hardness and this deviation was explained by precipitation which occurred during quenching.

The isothermal decomposition of the supersaturated solid solution of $\alpha + Fe_2Ta$ resulted in a sizeable hardness increase for the 2 at. pct tantalum alloy, but only a modest increase for the 1 at. pct alloy. The age hardening characteristics for these two alloys at aging temperatures of 600°C, 700°C, and 800°C are shown in Fig. 8. The age hardening behavior is characteristic of nucleation and growth with the peak hardness increasing and shifting to longer times with decreasing temperature. A single peak was always observed, indicating that the supersaturated solid solution decomposed by the following reaction:

$$\alpha(\text{supersat.}) = \alpha + Fe_2Ta$$

At a given temperature hardening begins at shorter times with increasing solute content, but the time to peak hardness does not shift. Also, the hardness shows an increase with increasing solute content at a constant temperature. Speich[3] found a shift in the time to peak hardness between 1 at. pct and 2.3 at. pct Nb alloys but this shift may have resulted from the precipitation which occurred during quenching in the 2.3 at. pct alloy, as noted in Fig. 7.

2) Second Phase Identification: Second phase particles extracted from a 2 at. pct Ta alloy aged 5 hours at 800°C were identified as the hexagonal Laves phase ($MgZn_2$ type, C14). The X-ray diffraction results are presented in Table I and were found to match the results for both Fe_7Ta_3 and Fe_5Ta_3 as listed in the ASTM Powder Diffraction File. However, the

results in Table I are closest to the interplanar spacings and intensities listed for Fe_7Ta_3.

The lattice parameters a_o and c_o and the c/a ratio were determined by a method of successive approximation as outlined by Massalski and King.[13] The resulting values are listed in Table II along with the results of other studies. Comparing a_o, c_o and c/a from this work to the values reported by Hansen it is seen that a_o is less while c_o and c/a are greater than Hansen's values. The lattice parameters reported by Hansen were obtained from stoichiometric Fe_2Ta, while the data from this work are from the Laves phase in equilibrium with α iron. The two methods of preparation would result in equal compositions if the Laves phase had no range of homogeneity, as suggested by Hansen, but it is more likely the Fe-Ta Laves phase has a range of homogeneity similar to the Fe-Nb Laves phase.[5] Goldschmidt [17,18] found that the Fe-Nb Laves phase had a difference in lattice parameters of Δa_o = + 0.021 A°, Δc_o = + 0.014 A° and $\Delta c/a$ = -0.004 when comparing compounds with 20 and 40 at. pct niobium. The a_o and c/a ratio for the Fe-Ta Laves phase in equilibrium with α iron vary in the same way from the stoichiometric values as does the Fe-Nb Laves phase. Also, it has been predicted by L. Brewer[7] that the Fe-Ta Laves phase is stable over a composition range of 25 at. pct to 35 at. pct tantalum. From the lattice parameter data for the compound Fe_2Ta in equilibrium with α iron, the expected similarities between the Fe-Ta and Fe-Nb systems and predictions by L. Brewer it is concluded that the Fe-Ta Laves phase exists over a range of composition. However, the limits of this range cannot be defined at this time.

3) Precipitate Morphology: The precipitate morphology in aged samples of the Fe-Ta alloys were quite similar to those found by Speich[3] for

Fe-Nb alloys. It was stated earlier that a single hardness peak indicated the absence of a metastable phase and this was supported by electron diffraction studies of 1 at. pct Ta aged 10 min. at 700°C and 2 at. pct Ta alloys aged 2 min. at 700°C. A comparison of these results with the X-ray diffraction results obtained from extracted particles is made in Table I. The precipitating sequence was grain boundary → dislocation → matrix and is demonstrated by Fig. 4 and Fig. 9. In Fig. 9a the aligned plate particles have formed at dislocations, whereas smaller random particles had formed in the matrix.

A peak aged sample exhibited a large amount of grain boundary phase with a small precipitate free zone adjacent to the boundary, as shown in Fig. 10. An electron beam microprobe analysis of the tantalum concentration at the grain boundary revealed the Laves phase network but not a tantalum depleted zone. Therefore, the precipitate free zone was believed to be the result of a low defect density adjacent to the boundary. A similar situation is found in the Al-Cu system where vacancy depletion near the grain boundary results in a precipitate free zone.

The nucleation of precipitates with a semi-coherent interface at dislocations has been discussed by Nicholson.[19] He postulated that the misfit vector of the precipitate and the burgers vector of the dislocation must be non-perpendicular, and this restriction results in certain habit planes being favored and others being excluded for a given burgers vector. The absence of one of the three possible habit planes for θ′ precipitates in Al-Cu alloys has been observed by Thomas and Nutting.[20]

Parallel arrays of plate particles in the Fe-Ta system have been observed as noted previously and shown in Fig. 9. Transmission microscopy

studies have shown that these plates formed with a $(100)_\alpha$ habit plane and exhibit interface coherency strain contrast, as shown in Fig. 11. Dislocation contrast at these arrays has not been conclusively shown. However, the strong particle strain contrast could obscure dislocation contrast. Analysis of electron diffraction patterns from these particles indicate that they are the hexagonal Laves phase, as shown in Table I. In Fe-Nb[3,21] and Fe-Ti alloys a $(110)_\alpha$ habit plane was the only observed habit plane relationship.

The selection of a habit plane can be affected by the precipitate matrix interfacial matchup, anisotropy of the elastic modulus and the angle between the burgers vector and the misfit vector. In the Fe-Ta alloys investigated it is not expected that the lower elastic modulus of iron in the [100] direction would overcome the favorable matching of the $(0004)_L$ and $(110)_\alpha$ planes as well as the smaller misfit vector-burgers vector angle for the $(110)_\alpha$ plane. A burgers vector in the [111] direction makes an angle of 36° with the misfit vector for a plate on the (110) plane where the misfit vector is normal to this plane. The burgers vector makes an angle of 54° with the misfit vector for a plate on a (100) plane with the misfit vector normal to this plane. The formation of plate shaped molybdenum rich clusters have been observed by Hornbogen[22] in Fe-Mo alloys, and the 10% mismatch between the iron and tantalum atoms would favor a plate shape cluster. The formation of GP zones have never been associated with dislocation nucleation thus it is not likely that the plate particles in the Fe-Ta system originated as GP zones. It is possible that these plate particles nucleated as a cubic phase, possibly the $MgCu_2$ type Laves phase, and subsequently transformed to the hexagonal

$MgZn_2$ type Laves phase. The alignment of the plate edges with the cubic axis, as shown in Fig. 11a, supports this hypothesis, although the lack of this reaction at sites other than dislocations is not easily explained.

The occurrence of the arrays of parallel plate particles was always accompanied by the observance of a high dislocation density in close proximity. The dislocations may have been nucleated by prismatic punching when the particles lost coherency by a mechanism described by Weatherly[23]. He found a critical misfit was required for this mechanism to operate with relaxation occurring when a dislocation was punched out followed by a buildup until another dislocation is punched out. The critical stress for this mechanism for plate particles is:

$$\tau_s = \frac{3}{2} G e^T$$

where τ_s is the shear stress, G the shear modulus and e^T is the total stress free transformation strain. A transformation strain greater than 2% is sufficient to cause loops to be punched out.

The fraction of precipitates which had formed at dislocations was observed to increase with increased solute content in the Fe-Ta system. This behavior has also been observed by Thomas[24] in aluminum alloys. The ratio of the activation energy for dislocation nucleation to that of homogeneous nucleation has been theoretically analyzed for an incoherent precipitate by Cahn[25] and he found that the ratio of the activation energy for dislocation nucleation to that of homogeneous nucleation decreases as both the magnitude of the burgers vector and the negative of the volume free energy change increase. Cahn assumed the particle nucleated as a bulge on a cylinder lying along the dislocation line, and that

the interface was incoherent. Although these assumptions are not completely satisfied for plate particles in Fe-Ta alloys it indicates the effect of the variables. Cahn's analysis indicates that on a given dislocation the nucleation rate and hence the number of particles would increase with supersaturation. In Fe-Ta alloys this reaction was auto-catalytic by the process of nucleation and growth of particles at a dislocation followed by punching of dislocations which acted as new nucleation sites. The rate of the auto-catalytic reaction is dependent on the nucleation rate and growth rate of the particles. If it is assumed the ratio of the growth rate of particles at dislocations to the growth rate of matrix particles is independent of composition, an increase in the auto-catalytic reaction to that of matrix precipitation can be predicted by an increase in supersaturation from Cahn's analysis. An increase of dislocation nucleated particles over matrix particles has been observed in 1 at. pct and 2 at. pct tantalum alloy, as shown in Fig. 9.

The habit plane of the matrix particles was not determined, but it is thought to be the $(110)_\alpha$, as in Fe-Nb and Fe-Ti alloys. Overaging at 700°C resulted in clusters of particles with precipitate free regions near these clusters. This clustering resulted from the auto-catalytic dislocation nucleation reaction. Particles which had formed randomly in the matrix had an elongated plate shape, whereas particles which had formed at dislocations had a square plate shape. It was concluded by Speich that the particle shape in the Fe-Nb and Fe-Ti systems became more spherical with increasing supersaturation. In Fe-Ta alloys this change of shape resulted from increased dislocation precipitation and it is proposed that this mechanism could account for the shape change observed in Fe-Nb and Fe-Ti alloys.

D. Mechanical Properties

In the aged condition the Fe-Ta alloys investigated had a large grain size (1 mm diameter) which was surrounded by a 2 micron thick network of the Laves phase. The matrix contained up to 7 vol pct of hard plate particles. A large grain size and heavy grain boundary network are both detrimental to ductile fracture, as the mechanical properties of these alloys showed. The fracture strengths of the Fe-Ta alloys studied are given in Table III, and a scanning electron micrograph of a typical fracture is shown in Fig. 13.

The transgranular cleavage fracture is thought to have initiated by cracking in the brittle grain boundary Laves phase. Ductile rupture in the precipitate free zone may also have contributed to the initiation of transgranular cleavage, as the material marked A in Fig. 13 had failed by ductile rupture. Hahn et al[26] have measured a fracture stress of 80,000 psi at room temperature for coarse grained ferrite with a 0.4 mm grain diameter. The fracture stress values observed in the present study are consistent with these results.

SUMMARY AND CONCLUSIONS

When an Fe-Ta alloys is quenched from the δ phase region to room temperature the final product is either equiaxed or acicular α. The acicular α structure was observed only in the hypoeutectoid composition and it was the result of the $\delta \rightarrow \gamma \rightarrow \alpha$ transformation. The final structure of quenched hypereutectoid alloys was equiaxed α with a large grain size and low dislocation density. Grain boundary precipitates formed in both 1 at. pct and 2 at. pct Ta alloys during quenching.

It was shown that the Fe-Ta Laves phase probably has a range of homogeneity, in contrast to the phase diagram shown by Hansen.[6] This conclusion is supported by X-ray lattice parameter measurements of the Laves phase in equilibrium with α iron, the similarities between the Fe-Ta and Fe-Nb compounds, and the compositional stability range predicted by L. Brewer.[7]

The decomposition kinetics of the supersaturated α solid solution exhibited typical nucleation and growth characteristics with a single aging peak. The peak hardness increased and shifted to longer times with decreasing temperatures. The sequence of precipitation sites for this decomposition was the following: grain boundaries, dislocations, and matrix. The precipitate particles were plate shaped, with square plate particles forming at dislocations with a $(100)_\alpha$ habit plane; matrix particles formed which were needlelike and thought to have a $(110)_\alpha$ habit. The dislocation nucleation reaction was auto-catalytic and more predominant with increasing supersaturation.

REFERENCES

1. E. Hornbogen: Precipitation from Iron-Base Alloys, G. R. Speich and J. B. Clark, Eds. Vol. 28, p.1, Gordon and Breach Science Publ., New York, 1965.

2. A. K. Sinha, R. A. Buckley and W. Hume-Rothery: JISI, 1967, Vol. 205, p. 191.

3. G. R. Speich: Trans. TMS-AIME, 1962, Vol. 224, p. 850.

4. G. Sasaki: Mechanical Properties of Laves Phases, Dec. 1970, Univ. of Calif., Lawrence Radiation Laboratory, UCRL-20301.

5. R. P. Elliott: Constitution of Binary Alloys, 1st Suppl., p. 255, McGraw-Hill Book Co., New York, 1965.

6. M. Hansen: Constitution of Binary Alloys, 2nd Ed., p. 720, McGraw-Hill Book Co., New York, 1958.

7. L. Brewer: High Strength Materials, V. F. Zackay, Ed., p. 12, John Wiley and Sons, Inc., New York, 1965.

8. A. K. Sinha and W. Hume-Rothery: JISI, 1967, Vol. 205, p. 671.

9. C. A. Dube, H. I. Aaronson and R. F. Mehl: Rev. Met., 1958, 55, p. 201.

10. H. I. Aaronson: Decomposition of Austenite by Diffusional Processes, V. F. Zackay and H. I. Aaronson, Ed., p. 387, Interscience Publishers, New York, 1962.

11. H. B. Aaron and H. I. Aaronson: Met. Trans., 1971, Vol. 1, p. 23.

12. W. B. Pearson: A Handbook of Lattice Spacings and Structures of Metals and Alloys, p. 632, Pergamon Press, 1958.

13. T. B. Massalski and H. W. King: J. Inst. of Metals, 1960-61 Vol. 89, p. 169.

14. K. Kuo: Acta Met., 1953, Vol. 1, p. 720.

15. R. P. Elliott: (1954), T. R. No. 1, Contract AF 18(600)-642, Project No. B053.

16. H. J. Walbaum: Z. Krist, 1941, A103, p. 391.

17. H. J. Goldschmidt: Research, 1957, 10, p. 289.

18. H. J. Goldschmidt: JISI, 1960, Vol. 194, p. 169.

19. R. B. Nicholson: Electron Microscopy and Strength of Crystals, p. 861, G. Thomas and J. Washburn, Eds., J. Wiley and Sons, New York, 1963.

20. G. Thomas and J. Nutting: Symposium on the Mechanism of Phase Transformations in Solids, p. 18, Institute of Metals, London, 1956.

21. R. M. Forbes Jones and D. R. F. West: JISI, 1970, Vol. 208, p. 270.

22. E. Hornbogen: JAP, 1961, Vol. 32, p. 135.

23. G. C. Weatherly, Phil. Mag., 17, 791 (1968).

24. G. Thomas, Phil. Mag., 4, 606 (1959)

25. J. W. Cahn, Acta Met. 5, 169 (1957)

26. G. T. Hahn, B. L. Averbach, W. S. Owen and M. Cohen: Fracture, B. L. Averbach, D. K. Felbeck, G. T. Hahn and D. A. Thomas, Eds., p. 98, The M. I. T. Press, Cambridge, Massachusetts, 1959.

Table I.

	X-Ray Diffraction Data Fe-2 at. pct Ta alloy aged 5 hr at 800°C		Electron Diffraction Data from thin foil aged 10 min at 700°C
hkl	d(A°)	I/I(11·2)	d(A°)
10·0	4.122	11	
00·2	3.893	5	
10·1	3.655	8	
10·2	2.838	8	
11·0	2.391	75	2.39
10·3	2.204	79	2.21
20·0	2.074	27	2.08
11·2	2.042	100	
20·1	2.006	63	
00·4	1.957	15	1.97
20·3	1.625	13	1.66
21·0	1.570	23	1.54
30·0	1.386	25	
21·3	1.347	47	
30·2, 00·6	1.307	43	
20·5	1.252	33	
22·0	1.201	33	

Table II. Lattice Parameter Data for the Compound Fe_2Ta

a_o (A^o)	C_o (A^o)	C/a	Reference
4.806	7.846	1.633	This work
4.828	7.838	1.624	6
4.816	7.868	1.633	14
4.817	7.822	1.624	15
4.81	7.85	1.63	16
4.80	7.84	1.63	ASTM Powder Diffraction File for Fe_7Ta_3.

Table III. Mechanical Properties of Peak Aged Samples

Composition at. % Ta	Treatment	Fracture Strength (ksi)
1	60 min - 700°C	58.0
2	7200 min - 600°C	48.0
2	60 min - 700°C	65.9
2	8 min - 800°C	47.8

FIGURE CAPTIONS

1. Iron rich portion of the Fe-Ta phase diagram. (Sinha, Hume-Rothery[8])
2a. Optical micrograph showing grain boundary allotriomorphs and intragranular idiomorphs in an Fe- 1 at. pct Ta alloy quenched from 1400°C.
2b. Optical micrograph showing a grain boundary allotriomorph in an Fe- 1 at. pct Ta alloy quenched from 1400°C.
3. Optical micrograph showing primary sawteeth in an Fe- 1 at. pct Ta alloy quenched from 1400°C.
4. Transmission electron micrograph showing Laves phase particles at prior δ grain boundary in an Fe- 1 at. pct Ta alloy quenched from 1400°C.
5. Schematic Time-Temperature-Transformation curves for Fe-Ta alloys. a) Hypoeutectoid composition. b) Hypereutectoid composition.
6. Lattice parameter of iron versus solute content for Fe-Ta and Fe-Nb alloys.
7. Hardness versus solute content for titanium, niobium and tantalum in BCC iron.
8. Hardness versus time at 600°C, 700°C and 800°C in a) Fe- 1 at. pct Ta alloy. b) Fe- 2 at. pct Ta alloy.
9. Carbon extraction replica showing Laves phase particles which have nucleated at a dislocation after aging 10 min at 700°C. a) Fe- 1 at. pct Ta alloy. b) Fe- 2 at. pct Ta alloy.
10. Scanning electron micrograph showing the grain boundary network of Laves phase in an Fe- 2 at. pct Ta alloy aged 90 min at 700°C. The surface was over etched with nital and tilted 30° in microscope.

11. Transmission electron micrograph showing Laves phase particles which have nucleated at a dislocation in an Fe- 1 at. pct Ta alloy aged 10 min at 700°C. a) Foil normal [200]. b) Foil normal [110].
12. Carbon extraction replica showing Laves phase morphology after aging 400 min at 700°C. a) Fe- 1 at. pct Ta alloy. b) Fe- 2 at. pct Ta alloy.
13. Scanning electron micrograph showing a fracture surface of an Fe- 2 at. pct Ta alloy aged 6 min at 800°C.

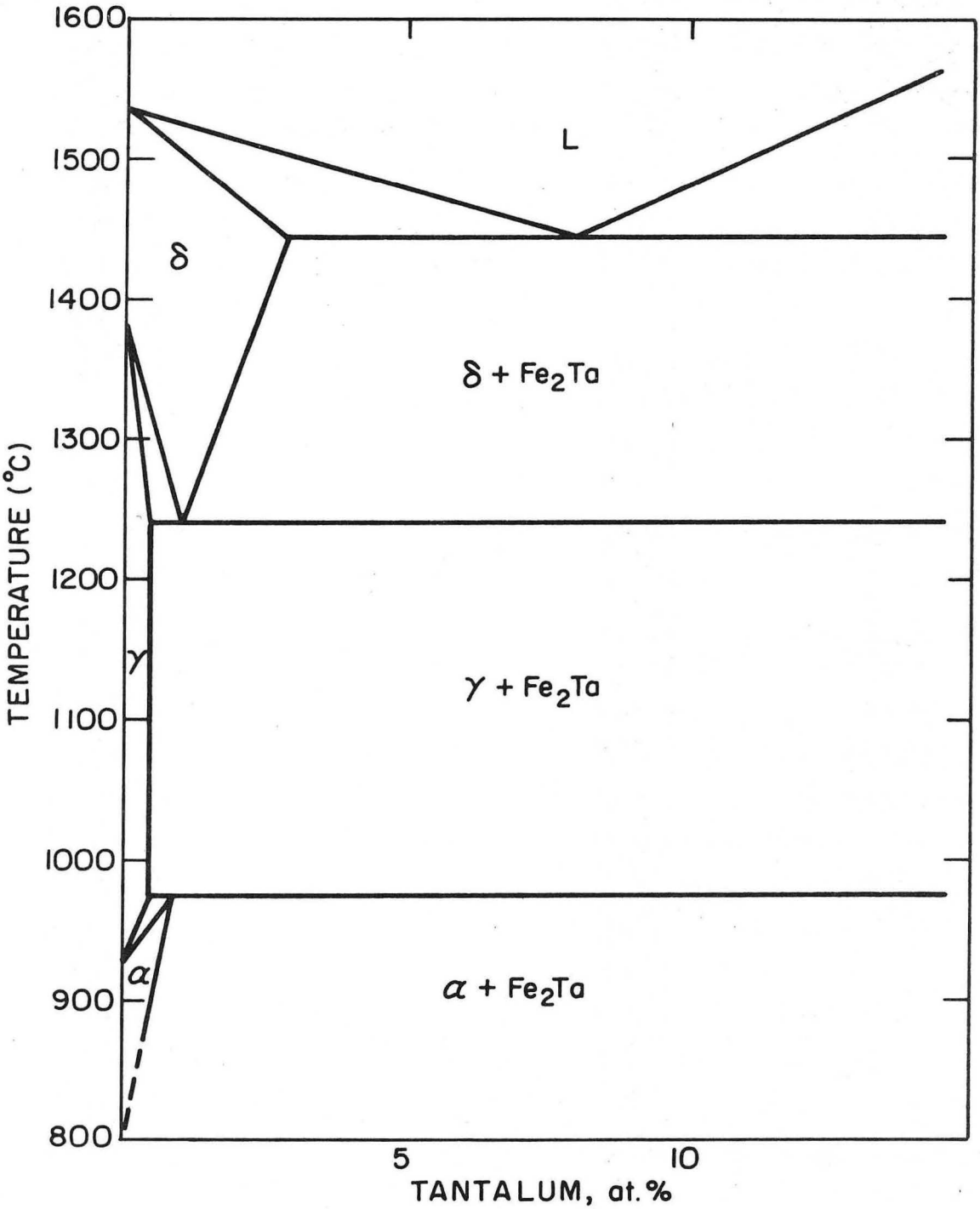

XBL 719-7223

Fig. 1

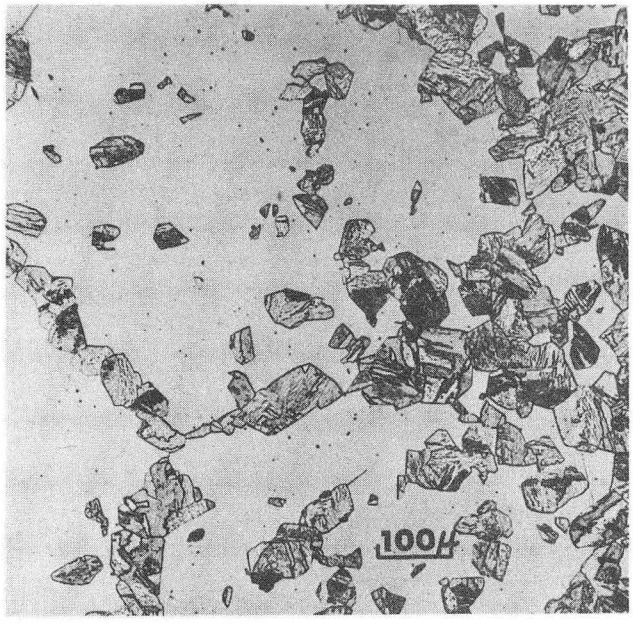

(a)

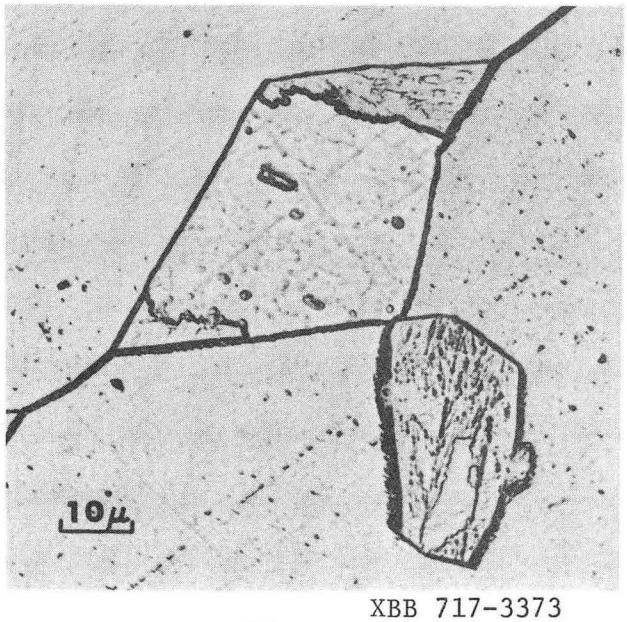

XBB 717-3373

(b)

Fig. 2

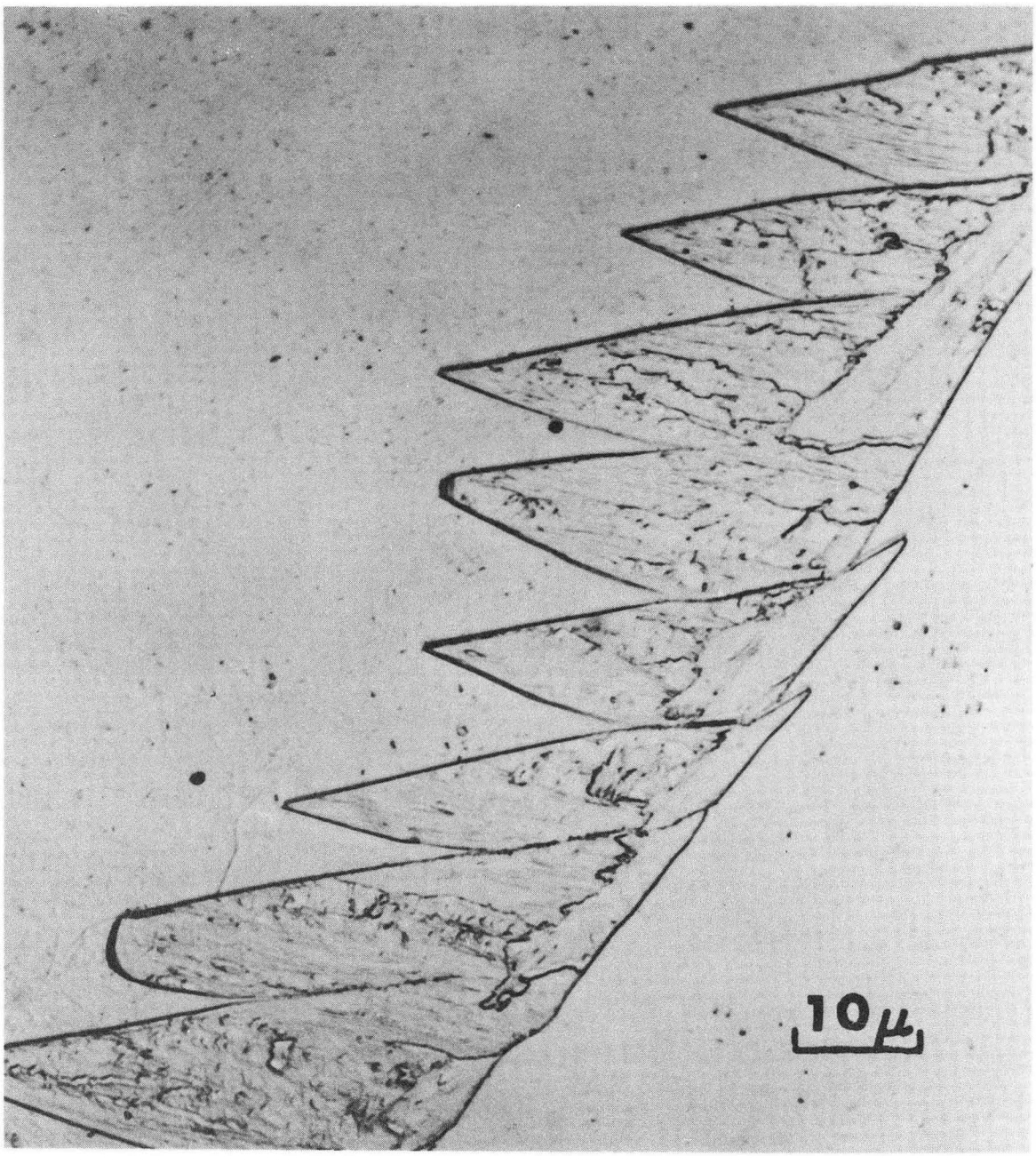

XBB 717-3370

Fig. 3

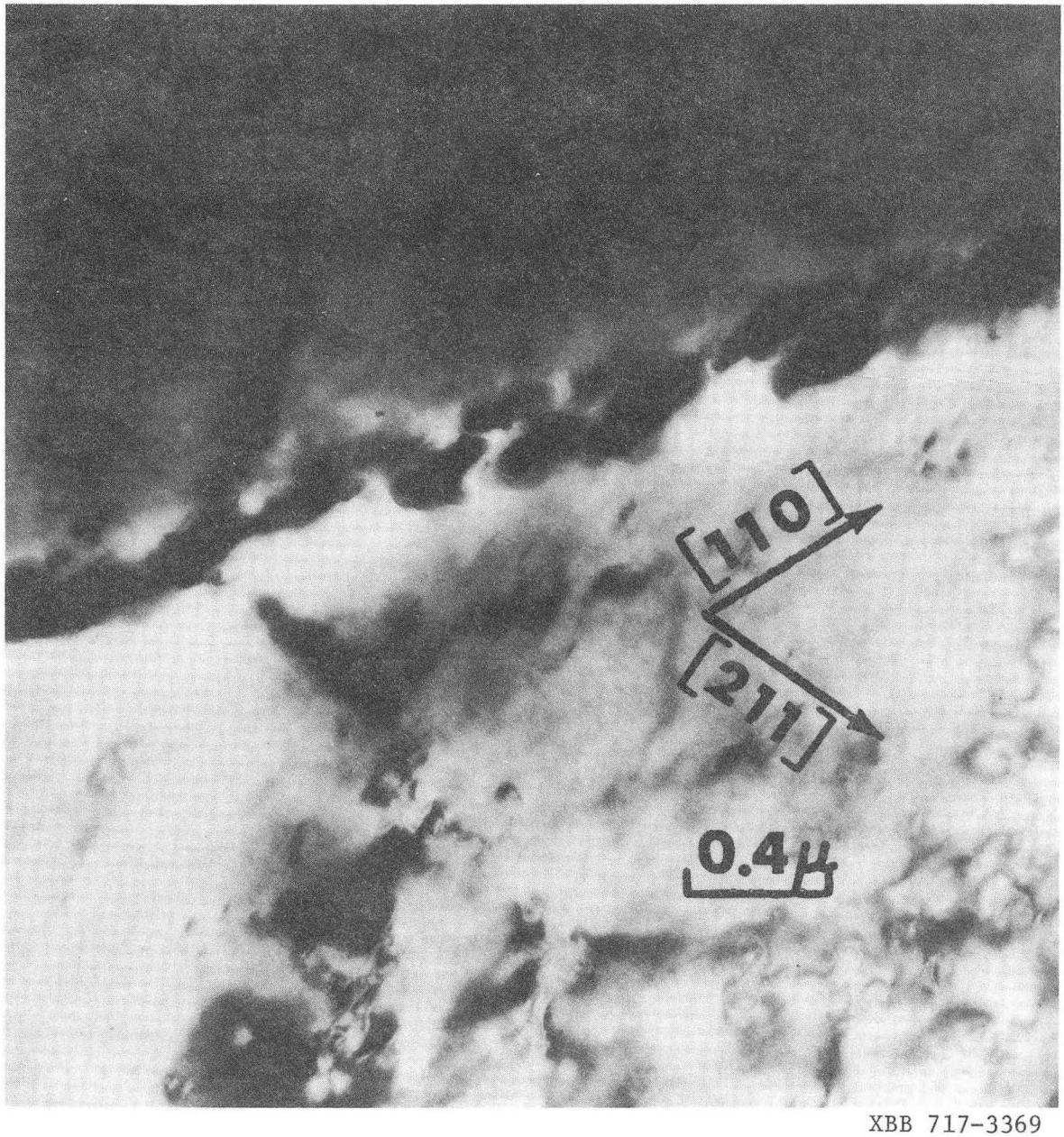

XBB 717-3369

Fig. 4

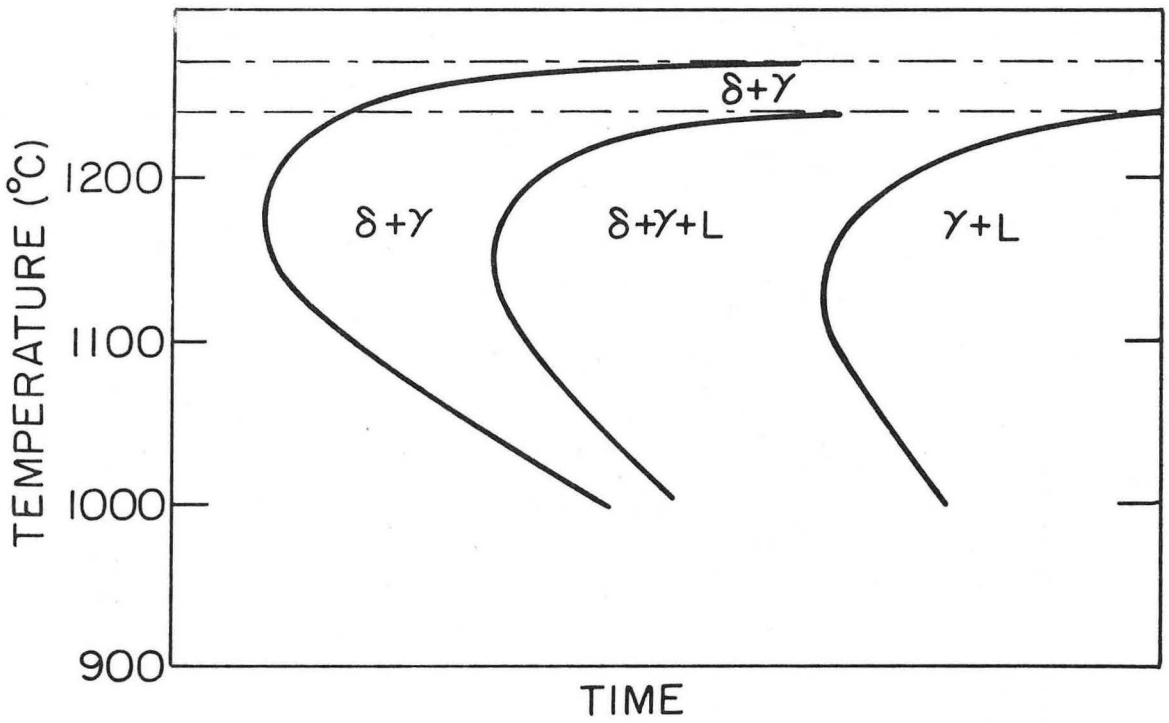

(a)

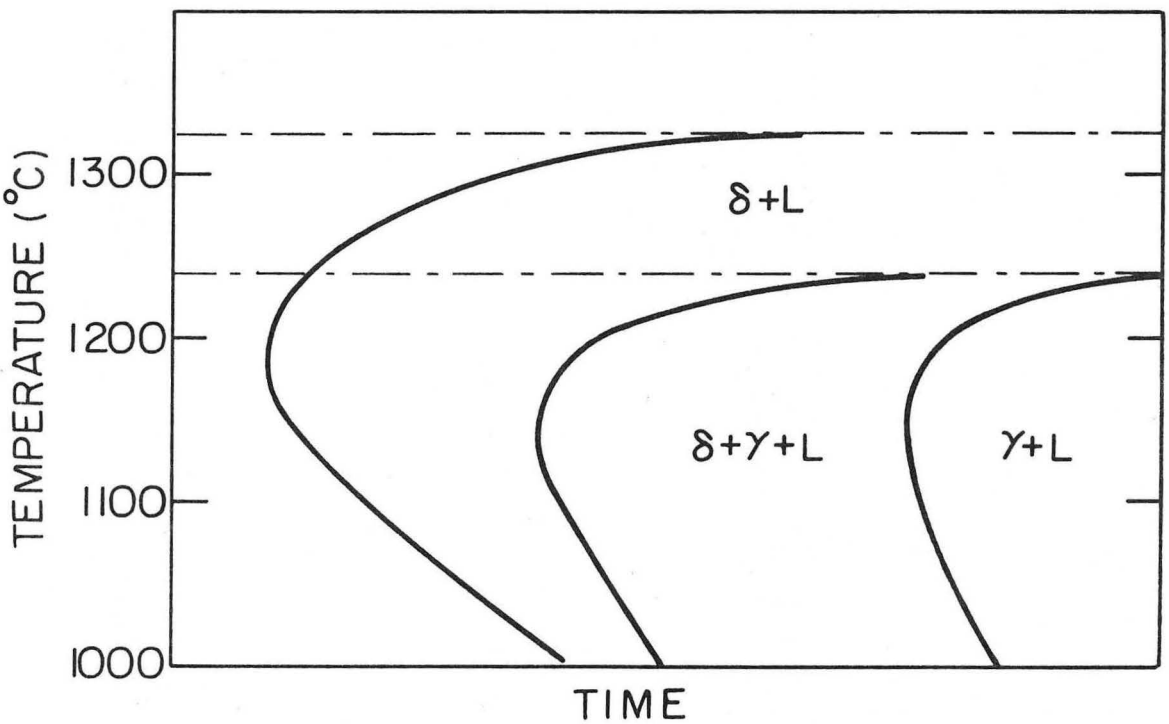

(b)

XBL 717-1211

Fig. 5

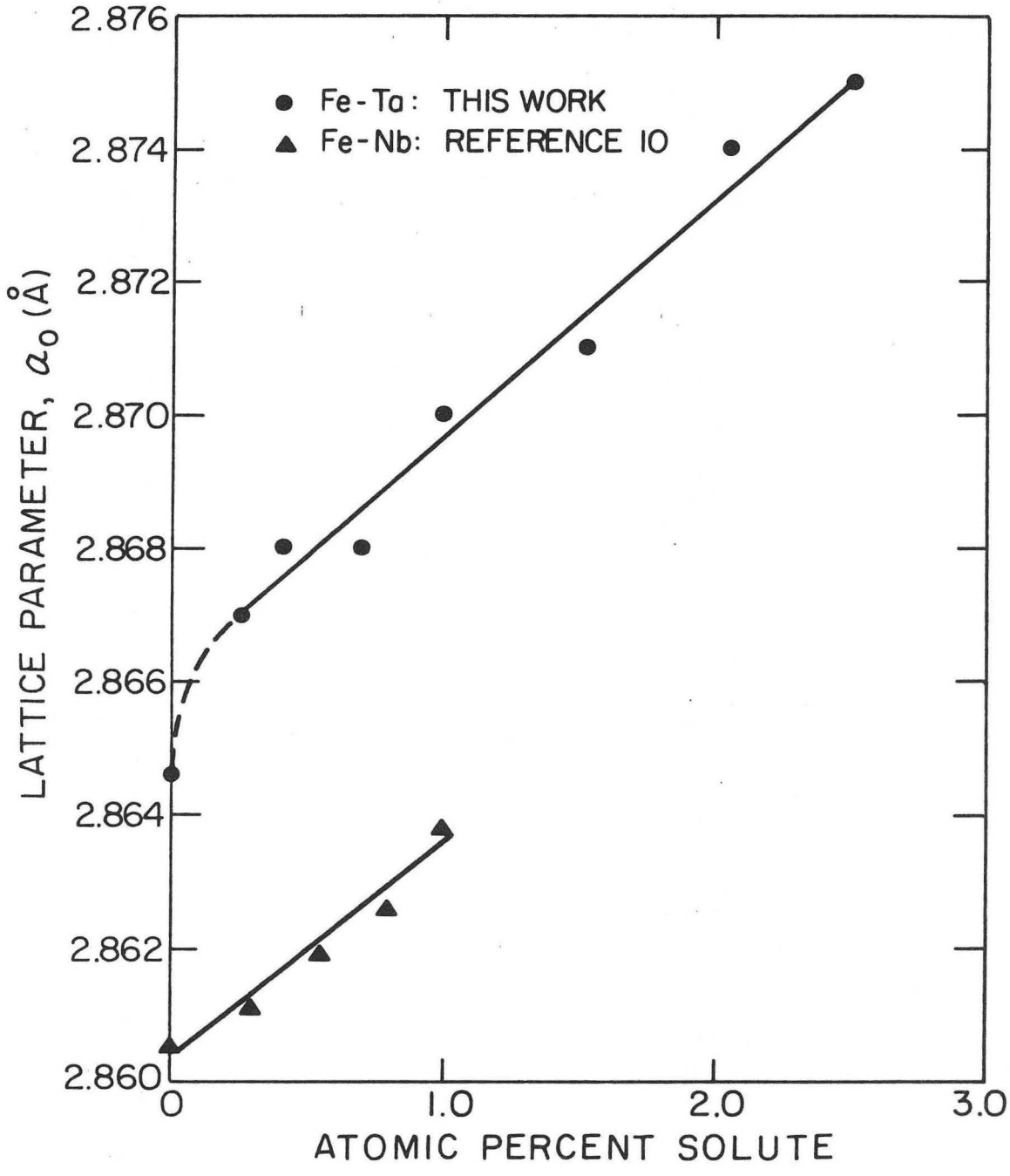
2.876
2.874
2.872
2.870
2.868
2.866
2.864
2.862
2.860
LATTICE PARAMETER, a_o (Å)
Fe-Ta: THIS WORK
Fe-Nb: REFERENCE 10
0
1.0
2.0
3.0
ATOMIC PERCENT SOLUTE
XBL 717-1212

Fig. 6

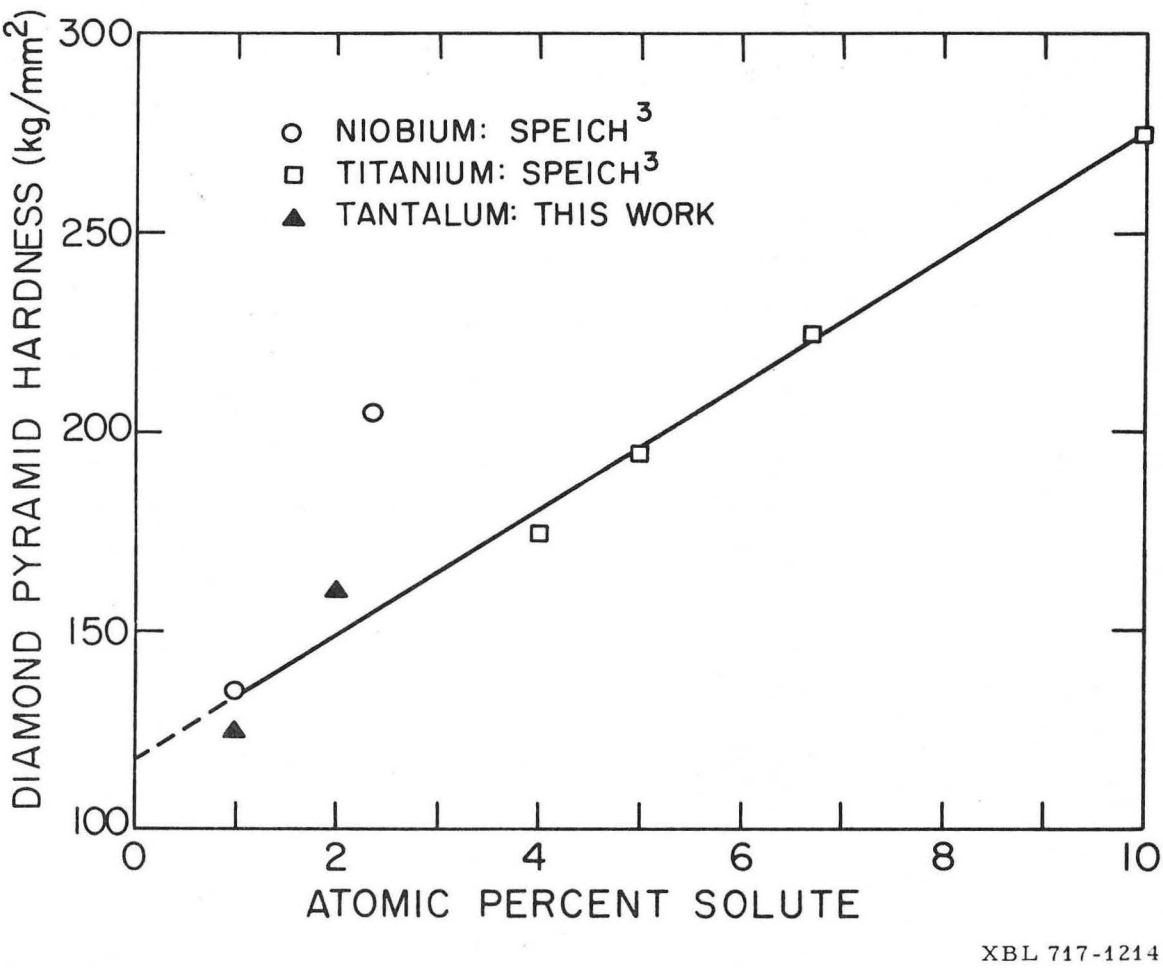

Fig. 7

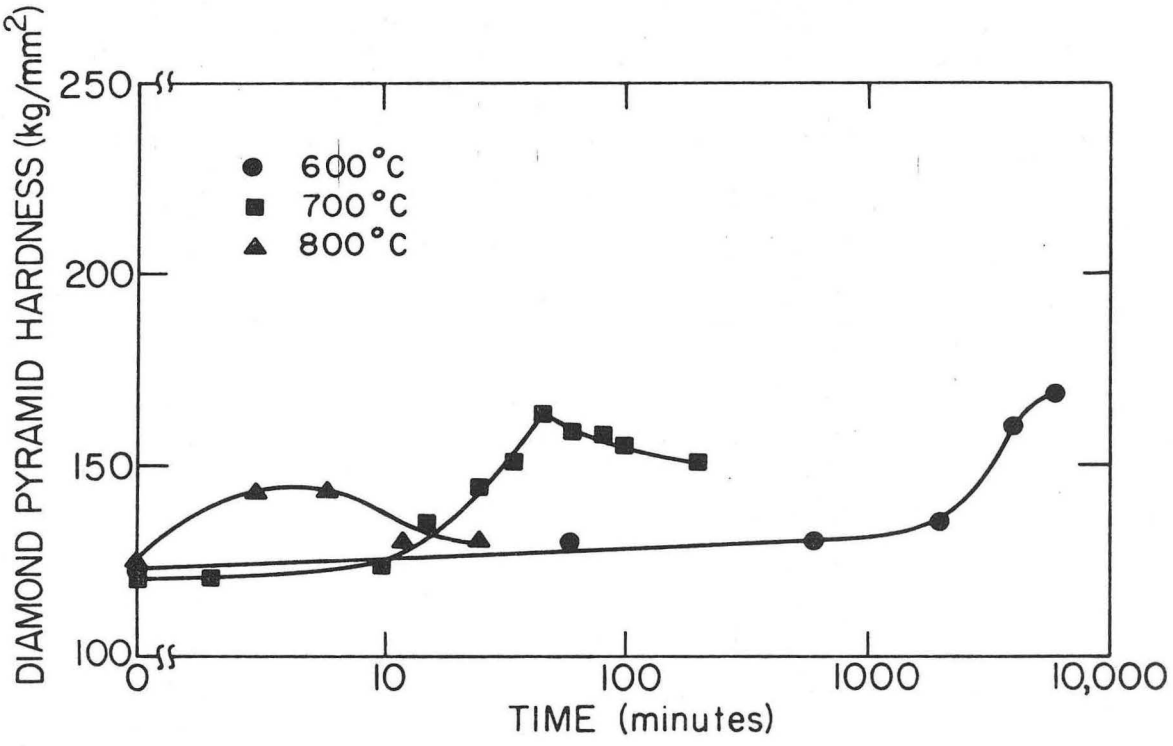

XBL 717-1213

Fig. 8a

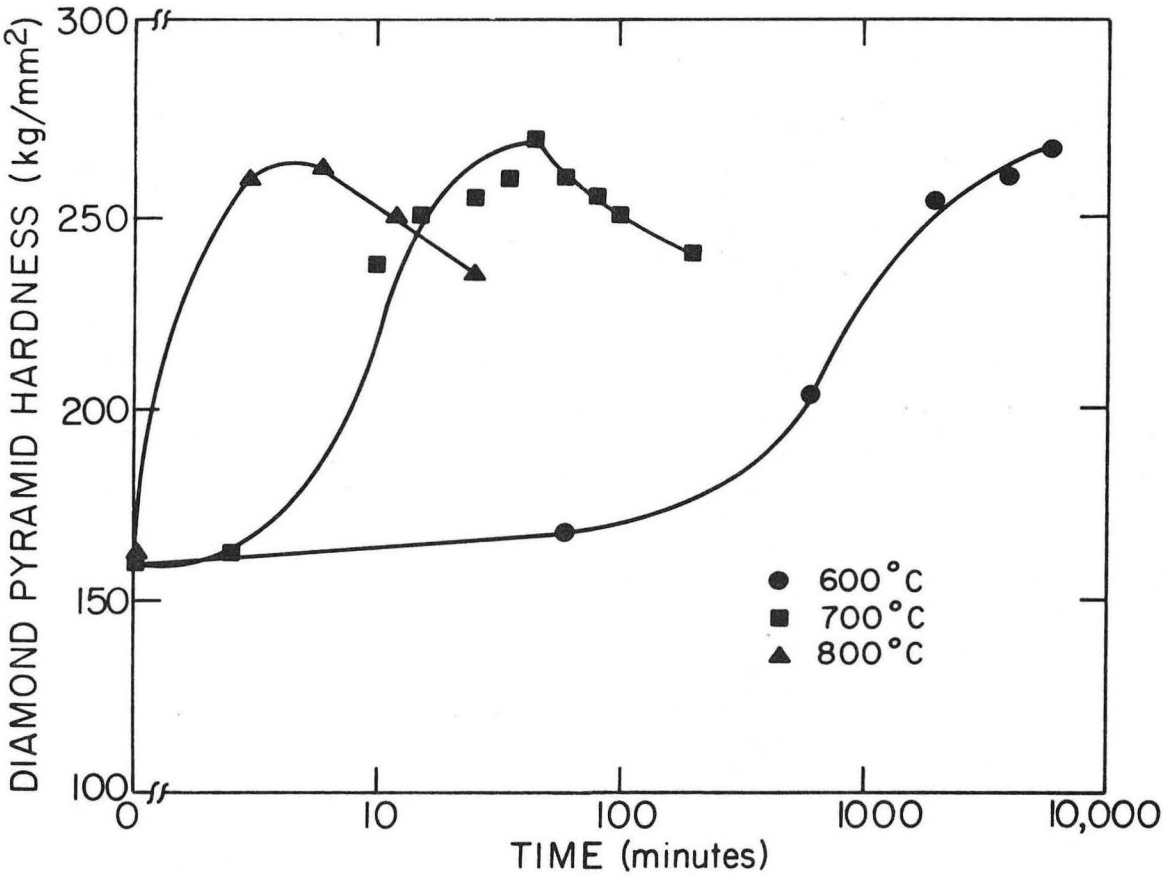

XBL 717-1215

Fig. 8b

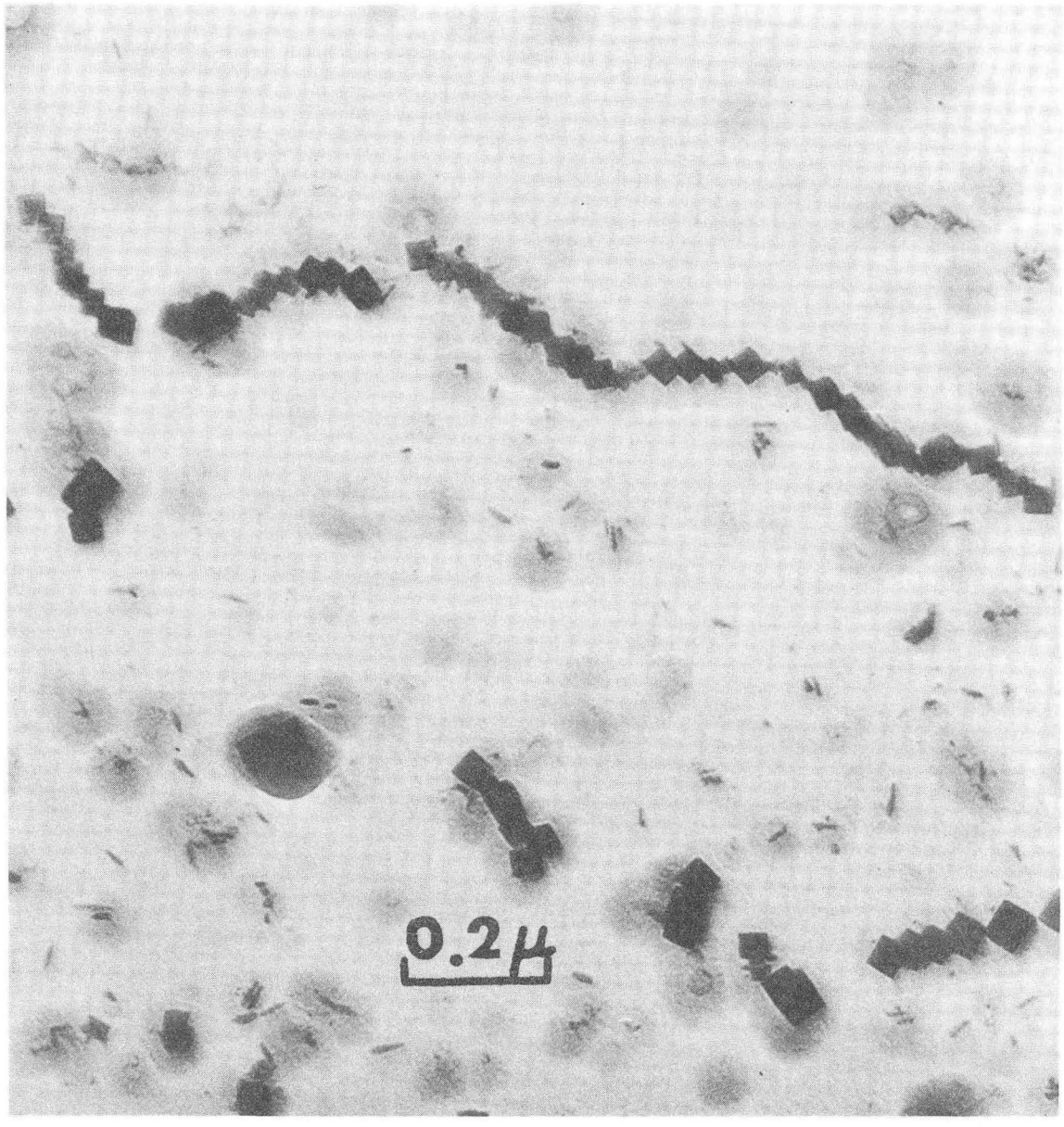

XBB 717-3365

Fig. 9a

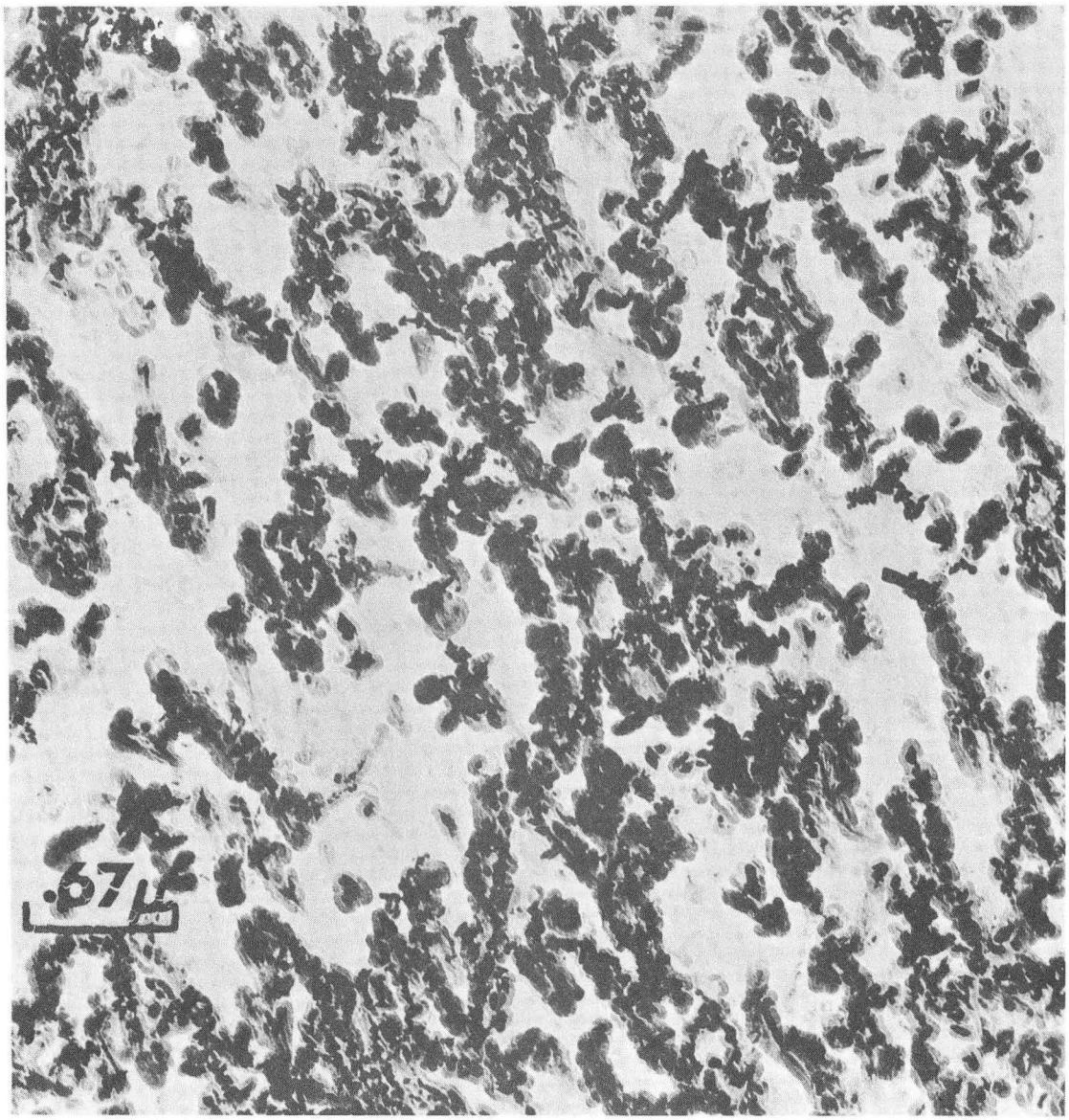

XBB 717-3366

Fig. 9b

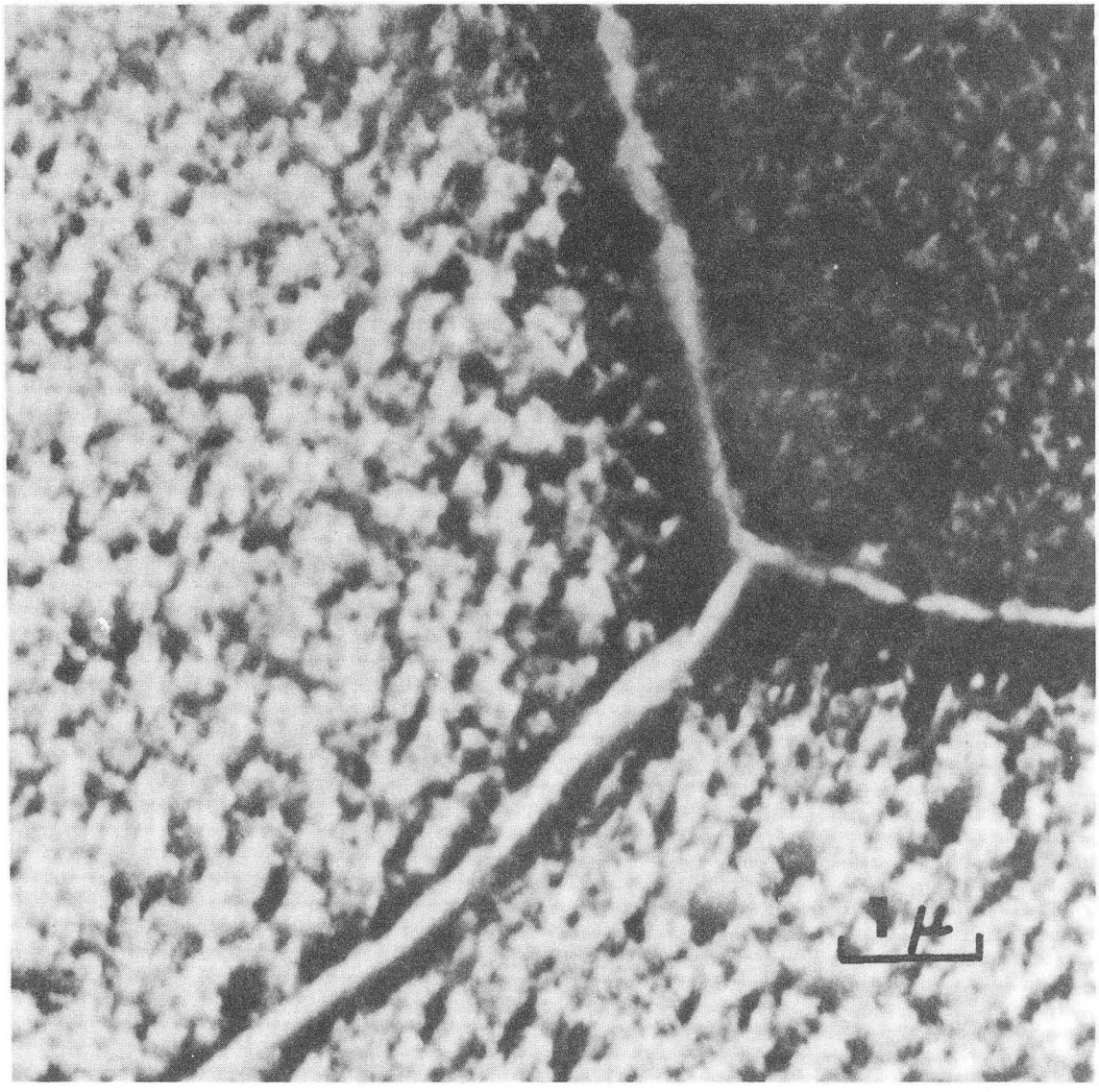

XBB 717-3367

Fig. 10

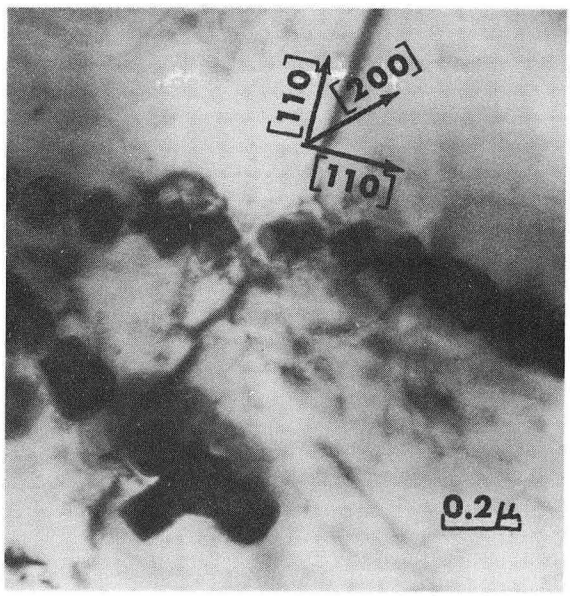

(a)

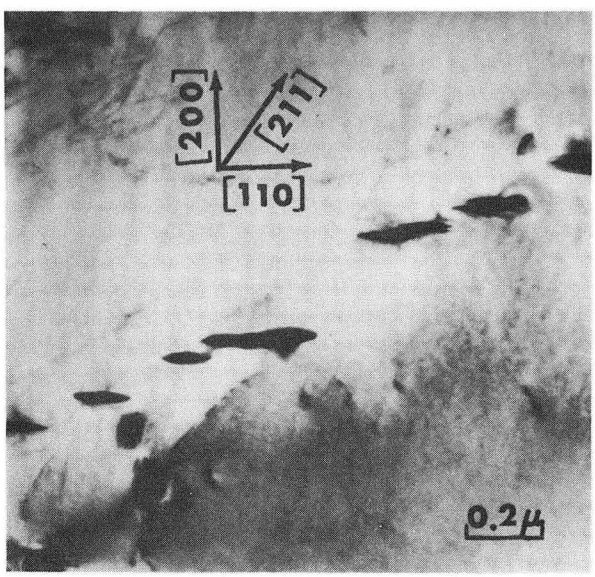

(b)

XBB 717-3371

Fig.11

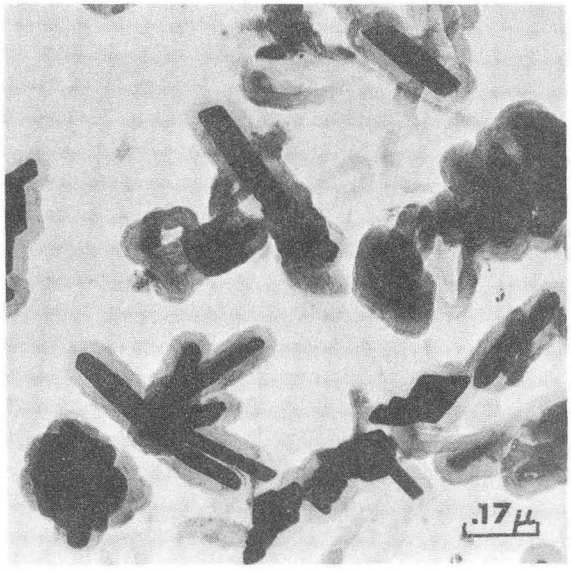

(a)

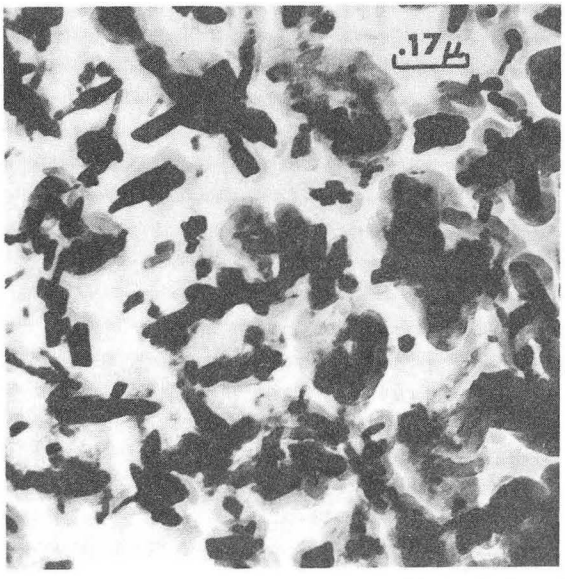

XBB 717-3372

(b)

Fig. 12

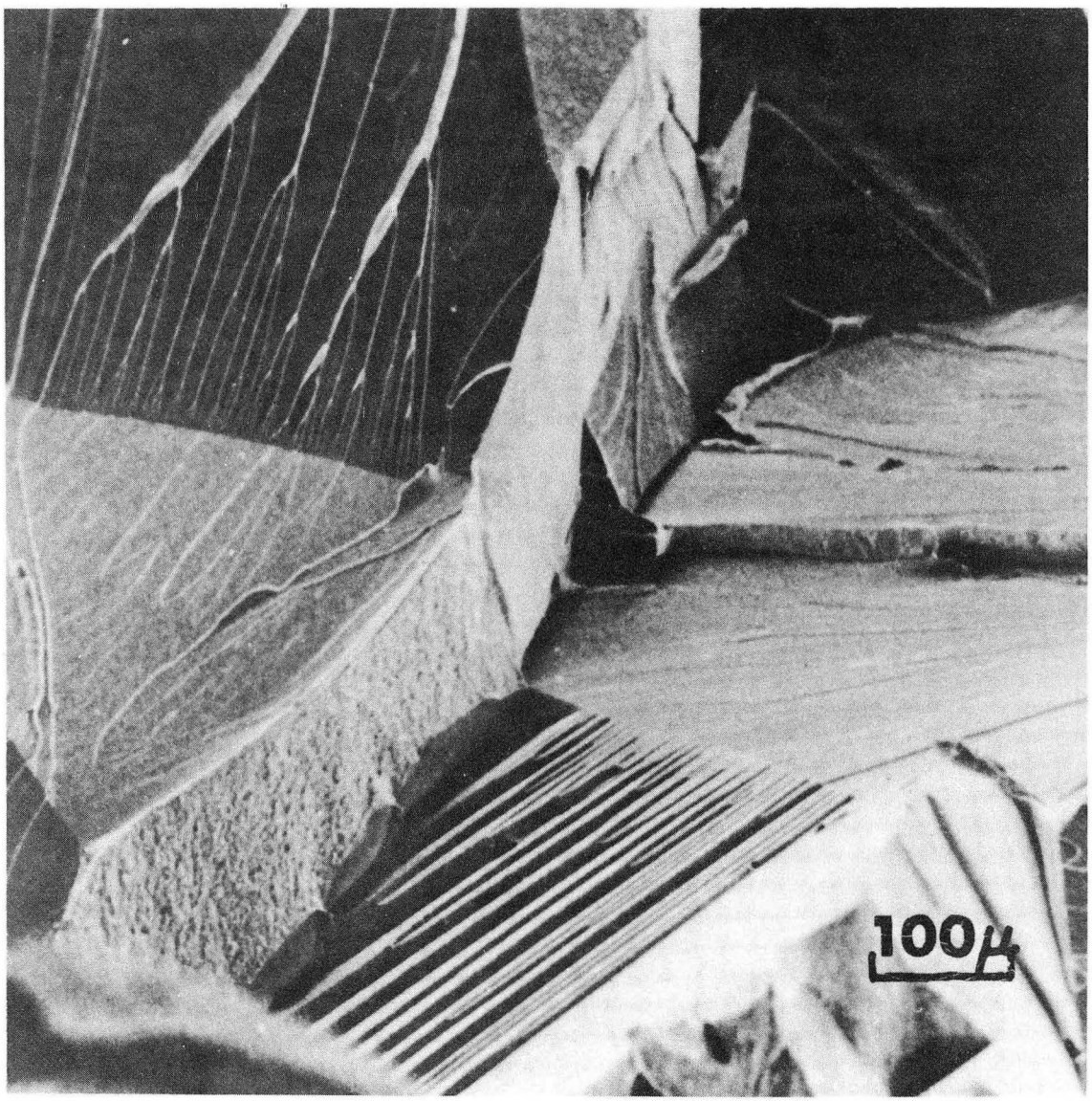

XBB 717-3368

Fig. 13

TECHNICAL INFORMATION DIVISION
LAWRENCE BERKELEY LABORATORY
UNIVERSITY OF CALIFORNIA
BERKELEY, CALIFORNIA 94720